Available online at www.sciencedirect.com

jmr&t Journal of Materials Research and Technology

journal homepage: www.elsevier.com/locate/jmrt

Original Article

Effects of steps on the load bearing capacity of 3D-printed single lap joints

Mohammad Reza Khosravani [a,*], *Payam Soltani* [b], *Tamara Reinicke* [a]

[a] *Chair of Product Development, University of Siegen, Paul-Bonatz-Str. 9-11, 57068 Siegen, Germany*
[b] *Centre of Engineering, Faculty of Computing, Engineering and the Built Environment, Birmingham City University, Birmingham, B4 7XG, United Kingdom*

ARTICLE INFO

Article history:
Received 21 November 2022
Accepted 4 January 2023
Available online 11 January 2023

Keywords:
Fracture
3D printing
Single lap joint
Finite element analysis
Adhesively bonded joints

ABSTRACT

Damage in adhesively bonded joints typically initiates in the overlap area due to high level of bonding (peel) stress. Different approaches are being considered to decrease the peel stress and improve the overall strength of the joint. One possible approach is to shape the over lap area into a stepped form configuration and enhance the performance of the joint. In the current study, we investigate effects of stepped-shape overlap area on the load bearing capacity of additively manufactured single-lap joints. To this aim, stepped-lap adhesively bonded joints with different designs and geometries in the overlap (bonding) area are considered with 3D-printed polylactic acid (PLA) adherends using the fused deposition modeling (FDM) process. Three configurations with different step sizes are considered to manufactured a set of adhesively bonded single-lap joints and to investigate the optimum length of the steps. The results are compared with our previous experimental findings on 3D-printed conventional single-lap joints. The obtained outcomes reveal that creating steps in the overlap area has a significant influence on the structural integrity and fracture load of 3D-printed adhesive-bonded joints and the bonded structures with identical step size in boding area reveal a better performance in load carrying capacity and shows a higher fracture load. Parallel to the experimental practices, a finite element model also developed to simulate the load carrying performance of the adhesively bonded single-lap joints with equal step size and 3D-printed PLA adherends. The FE model confirms the experimental outcomes and reveals the details of the cohesive failure and damage evolution mechanism in this bonded structures with PLA printed adherends. The proposed technique has a great potential to be a competitive alternative to conventional single-lap joints made by 3D printing. The presented results can be used for further fabrication of 3D-printed joints with a better structural performance.

* Corresponding author.
E-mail address: mohammadreza.khosravani@uni-siegen.de (M.R. Khosravani).

https://doi.org/10.1016/j.jmrt.2023.01.032

1. Introduction

Additive manufacturing (AM) as a rapid prototyping technique refers to adding raw materials during manufacturing which can be used to fabricate physical objects directly from computer-aided design (CAD) data. AM, also known as three-dimensional (3D) printing technology, is able to produce geometrically complex parts in a short period of time compared to traditional manufacturing processes [1]. 3D printing has been developing rapidly and dramatically and has attracted considerable attention in recent years. Considering various applications of additively manufactured parts, they have been utilized in a wide variety of applications such as soft robots [2], medicine [3], electronics [4], automotive [5], construction [6], food industry [7], aerospace [8] and nano-technology [9]. Based on various applications of 3D-printed parts, different engineering aspects have been investigated in this domain. For example, crushing performance [10], fracture behavior [11], machine learning [12], mechanical properties [13], creep properties [14], topology optimization [15], post-processing [16], mechanical strength [17], residual stress [18], impact behavior [19], and design optimization [20] have been studied in this field. According to ASTM 2792-12a [21], 3D printing has been classified into seven methods of which material extrusion is considered in the current study. Fused deposition modelling (FDM) technique is one of the most common and cost-effective methods in printing structures in which employs different types of filament and polylactic acid (PLA) amongst all types of filaments is considered as the most famous one. PLA is a biodegradable plant-based bio-polymer and PLA-based 3D-printed structures are more sustainable and more environmental friendly than any other common polymers used in FDM. Nowadays, commercial FDM printers are widely used in different industries and is considered as on of the main pillars of new generation of manufacturing technology. However, the maximum dimensions and volume of the final printed products are limited to the dimensions of the commercial 3D-printers (up to half a meter size in typical 3D printers), and this is considered as the inherent limitation of this manufacturing technique [22]. To tackle this challenge and benefit from the sustainable PLA 3D-printing process in manufacturing larger scale structures using commercial 3D printers, structures can be divided into and printed in smaller sub-structures in which can be assembled and bonded afterward. This would be an efficient and cost effective manufacturing method to create large size 3D-printed PLA structures without using giant untypical expensive 3D printers. However, in this technique, the integrity and mechanical performance of the assembled structure (with 3D-printed substructures) will very much dependent on the integrity and strength of the joints. Amongst different types of possible mechanical joints, adhesive joints are the best candidate in bonding 3D printed polymeric adhereds as they are easy to be implemented specially in complex geometries and also they are relatively considered as low price bonding method. Mechanical performance of adhesive bonded structures have been widely studied in literature with different types of adherends such as metallic [23–25], composite [26–28] materials and also joints with dissimilar adherends [29,30]. Single and double lap adhesive joints [31–33] and joints with different bonding configurations like stepped-lap joints [34,35] and scarf-joints [36,37] also considered to enhance the overall performance of adhesive bonding using different types of adherends.

Notwithstanding the large number of publications in different aspects of adhesive bonded joints, there are still limited number of research focusing on structural integrity, strength and performance of adhesive bonded joints with 3D-printed polymeric adherends. Mechanical performance of single-lap adhesive bonded joints with 3D-printed PLA adherends are studied in [38]. FDM printing technique is used to print the PLA adherend. Two different geometries (flat and sinusoidal shape) are considered in the overlap area along with two different printing orientations (flatwise and edgewise direction) for the PLA adherends. The results reveal the importance of the shape optimisation of the overlap area and printing orientation of adherends on the strength of the joint and enhancing its load capacity. Mechanical strength of single lap adhesive joints with PLA 3D-printed adherends also studied in [39]. This experimental study clearly shows that appropriate use of adhesive in structures with 3D-printed adherends not only does not weaken the load carrying capacity of the joints but in some cases might lead to slight enhancement of the maximum carrying force. Very recently, structural integrity, mechanical strength and fracture of adhesive bonded single lap joints with 3D-printed PLA adherends were studied both experimentally and numerically by the authors of this paper [40]. We could specify the optimum adhesive thickness and thanks to the 3D-computational model of the adhesive joints, stress distributions of adhesive and adherends within the bonding area were fully disclosed and corresponding cohesive failure modes were described. We could also show different printing parameters (i.e., different raster angle, raster width, and layer thickness) in manufacturing the adherends could have an impact on failure of the final adhesive single lap joints and might lead to change in failure mode from cohesive mode to fracture of the adherends. In another recent study [41], the authors of this paper focus on mechanical performance and fracture of single lap adhesive bonded joints with Polyethylene terephthalate glycol (PETG) printed adherends. FDM and different printing parameters are used to manufacture the substrate samples and an appropriate fast curing adhesive was employed to create the single lap joints. A set of standard tensile tests are conducted on the adhesive bonded joints with PETG adherends to analyse their mechanical strength, load carrying capacity and fracture modes. The experimental data are supported by a nonlinear 3D finite element model where the peel and sear stress distribution on adhesive layer are identified and cohesive failure of samples are predicted. We revealed that although all types of fracture modes can be seen in failure of these joints, proper choose of the adhesive layer thickness makes the cohesive failure the dominant failure mode and enhances the integrity of adhesive joints with 3D-printed PETG adherends.

In the present research, the impact of the morphology and configuration of the bonding area (over lap area) on mechanical performance and integrity of adhesive joints with 3D-printed adherends are investigated. A set of PLA adherends are

printed by FDM printers using the same printing parameters and with three different step configurations (with three different step lengths). So three sets of stepped-lap adhesive bonded joints (with different step length in the over lap area) are manufactured with the same adhesive type and optimum adhesive thickness. Standard tensile tests are conducted on joints to extract the mechanical performance and failure mode of the stepped-lap joint with different step length. In parallel, a 3D finite element model of these three types of stepped-lap adhesive bonded joints are used to investigate the performance of the joints with more details and provide an insight into stress distribution and load sharing within the overlap area and with different step sizes. To this end, we have organized the rest of this paper in the following way. Section 2, presents a brief overview of FDM process and its specifications. In Section 3, experimental investigations are described. Details of numerical simulations are presented in Section 4. In Section 5, the obtained results are presented and discussed. Finally, a short summary in Section 6 concludes the paper.

2. A brief overview of fracture in adhesive joints

Due to the developments in adhesive technology, the use of adhesively bonded joints has increased significantly. Categorisations of the different joints are based on their function, form or their location in the structure. Currently, there are many different types of adhesive joints, but the most common joint types are single-lap joints, double-lap joints, stepped-lap joints, and scarf joints [42]. In adhesive joints, there are different failure modes which are determined by the quality of the bond at each interface, specimen geometry, and loading. Fig. 1 shows schematics of several failure modes in adhesively bonded joints. Literature investigation confirmed that there are several parameters (e.g., surface preparation, adhesive thickness, joint configuration, adhesive properties, and environmental factors) which have significant effects on the strength of the adhesively bonded joints [43–45]. For instance, in [46] influence of surface patterns on the fracture behavior of adhesively bonded joint has been investigated. Later, effects of the temperature on the fracture properties of adhesive joints were analyzed in [47]. In this context, three different temperatures were considered and the fracture properties of a structural adhesive were examined. The obtained results indicated that the values for critical strain energy release rate decreased with the increase of the temperature.

The technical condition of the joint influences the stiffness of the whole structure and its load-bearing capability. A review of the literature reveals that several investigations were performed to study improvement of strength in adhesively bonded joints. Fig. 2 illustrates the classification of techniques that have been used to improve the strength of adhesive joint. For example, mixed-adhesive joints (combining two adhesives in a single joint) is considered as an alternative to the use of a single flexible adhesive which can reduce the stress concentration in the adhesive [48]. As depicted in Fig. 2, transverse adherend toughening is a method to improve strength of adhesive joints. This toughening can be performed by adding metal layers to increased transverse strength on the critical surface region [49], or using polymers to reduce delamination in adhesive joints [50]. Transverse joint reinforcement is another way to avoid delamination in adhesive joints. The reinforcement can be continuous threads as in stitched laminates, braiding [51], and 3D weaving [52], or it can be discontinuous rods or pins as in Z-reinforcement materials, such as Z-pins [53] and interleafing [54]. Although these techniques are very useful in preventing delamination in adhesive joints, transverse reinforcements has negative effect on the elastic modulus and strength of the materials. Therefore, currently optimization of configuration is considered as an effective method to improve strength of the joints.

The geometrical configuration has a crucial role on the structural integrity of the joint with effects on the adherends and the adhesive layer. In the design phase, it is very important to ensure that the joint geometry is carefully selected to avoid undesirable stresses. After determining global configuration of the joint, further improvement in the strength can be performed by local geometry modification. This includes the local modification of adherends, adhesive, and the combination of them. In single-lap joints, the load transfer is uneven along the overlap, which leads to stress concentration at the ends of the overlap. In the context of geometry design, a higher joint strength can be obtained by double-lap joints, stepped-lap joints, scarf-lap joints, and tapered-lap joints. It is noteworthy that strength improvement is usually accompanied by increased manufacturing difficulty. In the current study, stepped-lap joint is considered as a technique for strength improvement of 3D-printed joint which is described in the following section.

3. Experimental procedure

3.1. *Design and printing of specimens*

In order to determine basic mechanical properties, we have designed and examined dumbbell-shaped specimens made by PLA material in our previous study [40], where we investigated structural integrity of 3D-printed single lap joints. In this context, dumbbell-shaped test coupons tested according to ASTM D638 [55]. Schematic of tensile test and specimen geometry are illustrated in Fig. 3. As the same material is used in the current study, we refer to the documented basic mechanical properties.

In the present study, stepped-lap joint are designed, fabricated, examined to compare their strength with single-lap joints fabricated by the same material and process. Indeed, in our previous study [40] we used PLA material to printed single-lap joint specimens and investigate their structural integrity. In the current study, we used the same material and the step-joint specimens are printed under the same conditions and printing parameters to determine effects of steps in improving strength of the joints. Table 1 summarizes the material properties of utilized PLA based on the data sheet [56], and printing parameters documented during the printing process. It should be noted that the printing parameters were kept constant in fabrication of all specimens to ensure consistent printing quality.

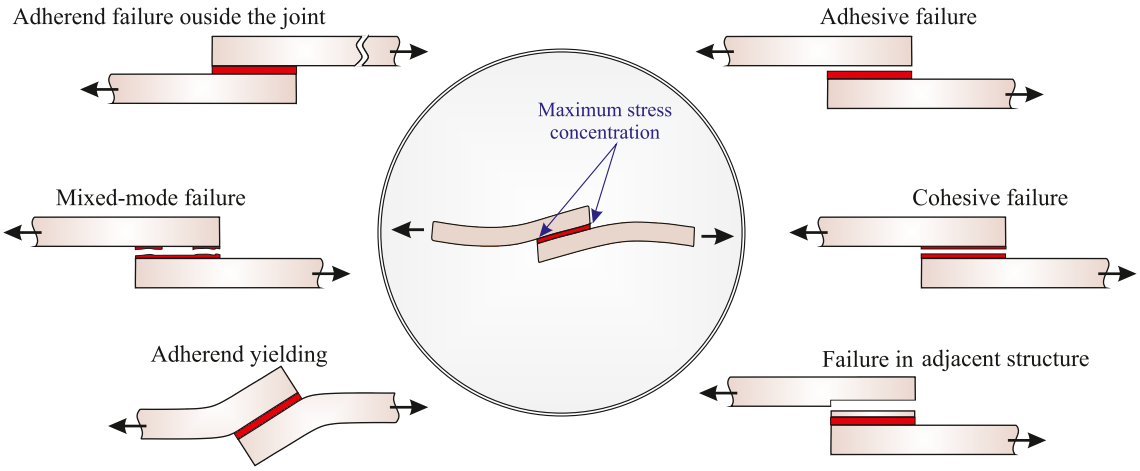

Fig. 1 – Schematics of different failure modes in adhesively bonded joints.

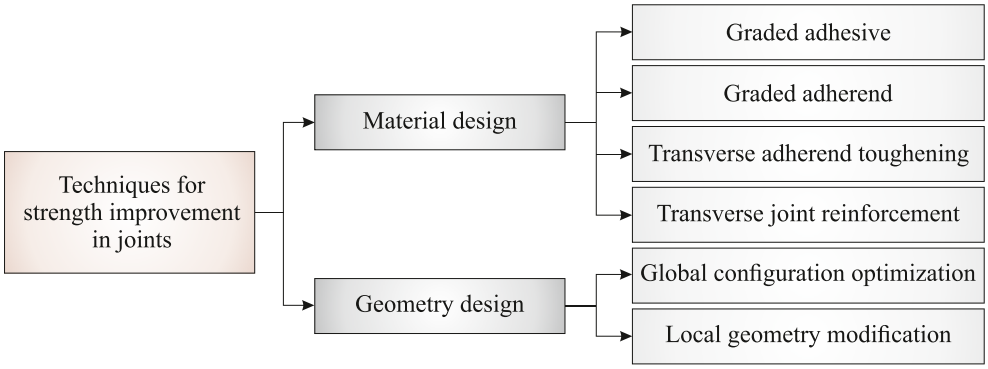

Fig. 2 – Classification of techniques to improve strength in adhesive joints.

All specimens are first drawn in a CAD platform and then saved as '. stl' format. The CAD files of specimens are used to extrude and deposit molten thermoplastic which is built up in layers from a horizontal base. Here, the files were imported to Cura™ slicing engine which is an open-source program for slicing and setting printing parameters. According to ASTM D3163-01 [57] single-lap joints are made with overlap region about one-quarter of the specimen length. In the current study, different step lengths are considered to investigate effects of step length on the structural integrity of the bonded joints. Geometry details of steps are as follows: (a) Design I: three steps with equal lengths, (b) Design II: largest step is in the middle, and (c) Design III: smallest step is in the middle. The thickness and width of the steps were kept constant in all specimens. Schematics of a conventional single-lap joint and geometrical parameters of modified joint with three steps are illustrated in Fig. 4. It is noteworthy that six specimens for each configuration (step length) were examined to confirm the repeatability and produce representative results. In order to ensure printing quality of the specimens, visual appearance of 3D-printed step-lap joints parts were investigated and failed parts were replaced.

Since type of adhesive and its properties has crucial roles on the bond strength of the adhesively bonded joints, selection of adhesive has become of significant importance. In the

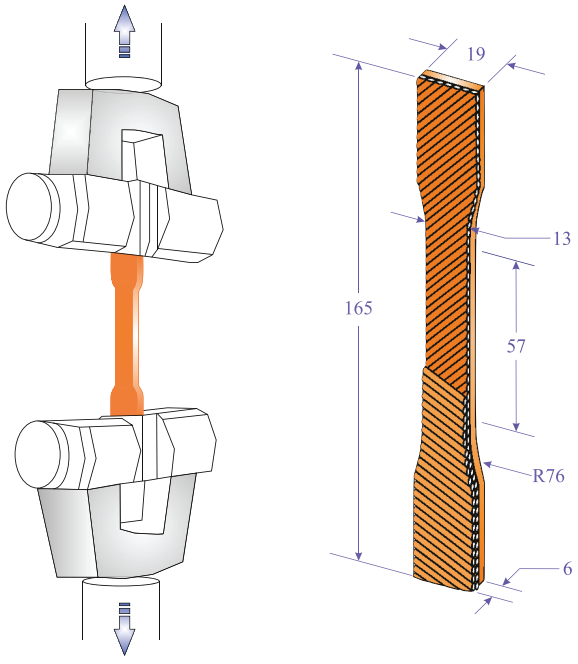

Fig. 3 – Schematics of tensile test and geometries of a dumbbell-shaped test coupon (dimensions in mm).

Table 1 – Printing parameters and properties of utilized PLA material.

Printing parameters	Values	PLA parameters	Values
Raster angle (°)	±45°	Density (gr/cm^3)	1.21
Raster width (mm)	0.75	Melting point (°C)	~ 160
Number of contours	2	Glass transition (°C)	~ 65
Infill percentage (%)	100	Elongation at yield (%)	2
Layer thickness (mm)	0.2	Elongation at break (%)	6
Bed temperature (°C)	55	Filament diameter (mm)	1.75
Nozzle diameter (mm)	0.8	Diameter tolerance (mm)	±0.05
Printing speed (mm/s)	30	Moisture absorption (ppm)	1968
Nozzle temperature (°C)	215	Izod impact strength (kJ/m^2)	5.1

present study, we used an industrial grade epoxy adhesive which is two components adhesive LOCTITE® EA 9466™ from Henkel (Düsseldorf, Germany) to bond 3D-printed parts and finish fabrication of test coupons. The use of robust experimental procedures is essential for the accuracy of the obtained results. It is worth mentioning that for the final phase of the specimen preparation we have designed and fabricated a fixture to maintain the alignment of the two parts of the 3D-printed step-lap joints during the curing period. In addition, as thickness of the adhesive has an important role in the mechanical performance of the bonded joints, it is necessary to keep the desired adhesive thickness. The utilized fixture was able to make the thickness of the adhesive layer precisely adjustable. Fig. 5 shows an exploded view of the fabricated fixture. All 3D-printed parts were cleaned, washed, and subsequently dried prior using the adhesive.

According to the technical datasheet of adhesive manufacturer, it was necessary to keep assembled parts from moving during cure. The adhesive cured at room temperature for 24 h according to the manufacturer's datasheet. Prior to the mechanical tests, geometry and appearance of the specimens were visually checked to ensure that there is no damage or defect in the specimens.

3.2. *Lap shear tests*

A series of lap shear tests was performed to analyze the failure behavior and strength improvement in 3D-printed step-lap

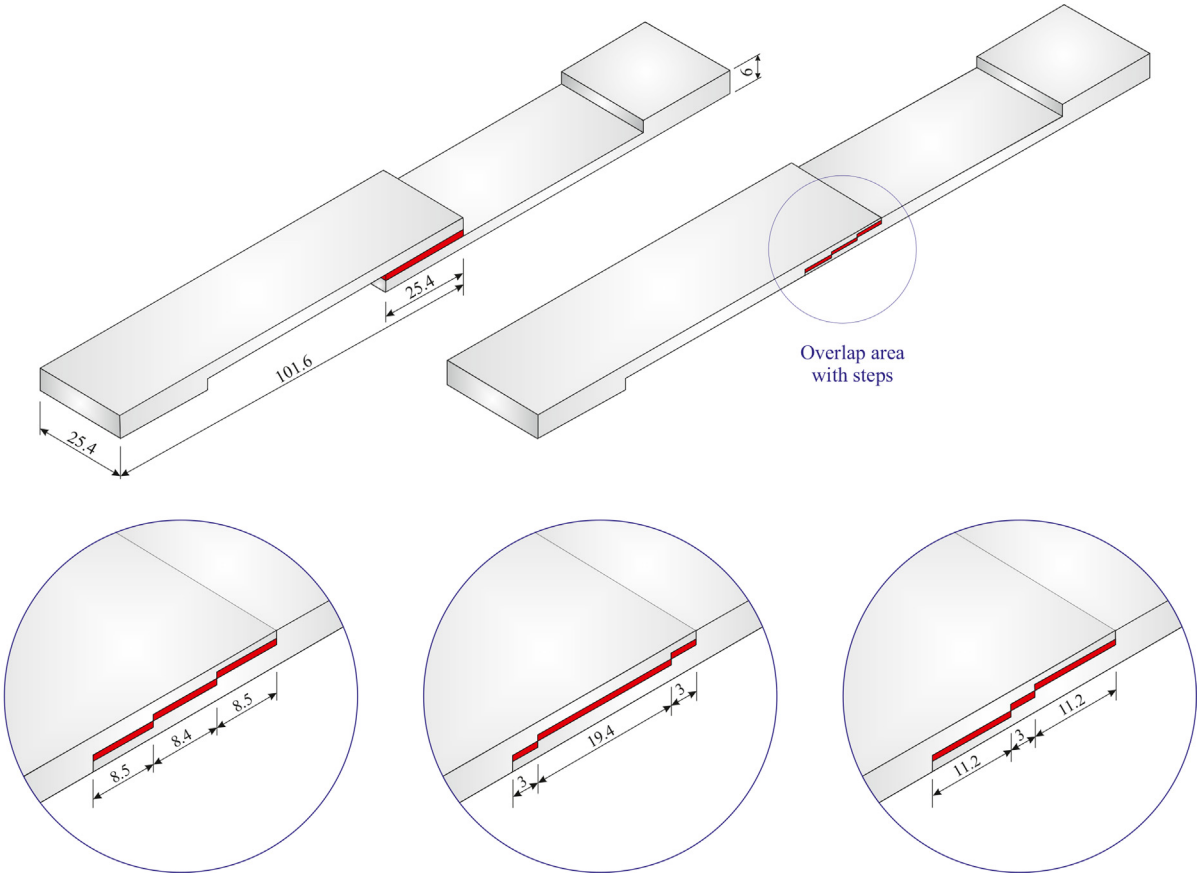

Fig. 4 – The conventional single-lap joint and geometry details in a modified joint with steps (dimensions in mm).

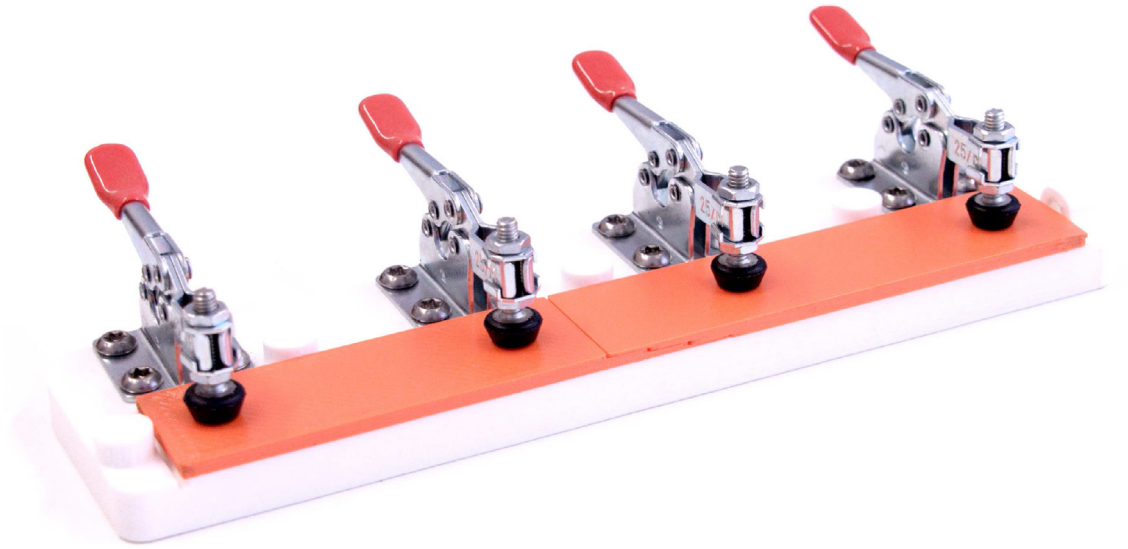

Fig. 5 – The fabricated fixture keeps a 3D-printed step-lap join.

joints. In this context, all tests were carried out using a hydraulic tensile test machine equipped with a 15 kN load cell. The step-lap joints were examined longitudinally along the machine axis which were pulled up to breaking of samples. The specimens were attached with the tensile machine cross heads grips that were inserted. The load was set according to the load cell as prescribed in machine. Displacement was measured by an encoding sensor. The machine has cross-head speed range of 0.01 mm/s to 30 mm/s and the series of static tensile test were performed under displacement control via constant cross-head movement of 1 mm/min. As the physical properties of materials can be affected by ambient temperature, all tensile tests were performed according to the standards for room temperature. In detail, the room conditions for tests of step-lap joints were 23 ± 3 °C and 50 ± 5% temperature and relative humidity, respectively. Fig. 6 shows a step-lap joint under test conditions.

Since overstress loads in adhesively bonded joints lead to failure, different failure modes can occur based on several parameters such as joint configuration, quality of bond at each interface, and loading. In the present study, we examined four specimens for each step configuration and different failure modes are occurred. The dominant failure mode observed among all examined specimens is the cohesive failure. Indeed, there are nine cohesive failure modes, along with one adhesive failure in tested samples. In addition, failure in adjacent structure is occurred in two specimens. The maximum fracture load belongs to cohesive failure mode and was equal to 2856.3 N. Fracture loads of each joint type are summarized in Table 2.

Cohesive failure shows a 'good' adhesive bond, because it indicates suitable adhesive curing conditions and good cohesive strength. In fact, cohesive failure within the adhesive is the preferred type of failure, because with this type, the maximum strength of the materials in the joint has been reached [58,59]. Moreover, cohesive failure mode is the desired mode of failure, because energy dissipation occurs primarily in the adhesive substrate. In addition, in the

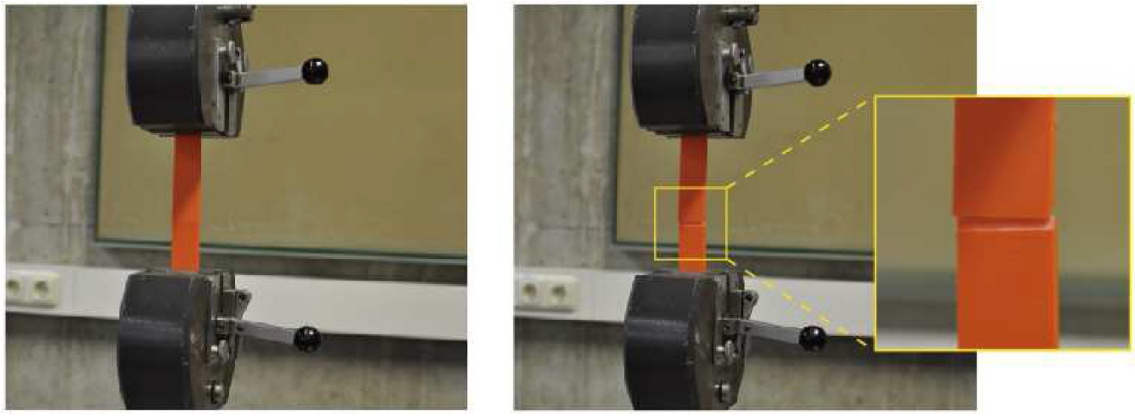

Fig. 6 – Additively manufactured step-lap joint, before (left), and after (right) tensile test.

Table 2 – The experimental failure loads of the examined 3D-printed step-lap joints.

Steps configuration	P_1 (N)	P_2 (N)	P_3 (N)	P_4 (N)	P_{avg} (N)
Design I	2652.4	2615.4	2856.3	2771.8	2723.9
Design II	1832.7	2052.8	2142.5	1919.1	1986.7
Design III	2073.6	1703.2	1814.3	1679.5	1817.6

cohesive failure, repair of the parts can be performed in a cost-effective manner which is another advantage of this failure mode. As discussed in [60,61], in analyzing an adhesive joint that has been tested to destruction, the mode of failure is often expressed as a percentage cohesive or adhesive failure. The ideal mode of failure is a 100% cohesive failure in the adhesive layer. Here, this type of failure is occurred in nine specimens.

Information about failure mode is beneficial for determining cause of failure, but it should not be used as a sole criterion for evaluation of the joints. According to the tests on step-lap joints, force-displacement curves (for highest fracture loads in each design) and corresponding stress-strain relationship of examined joints are determined and illustrated in Fig. 7. As it shown, the higher slope (higher stiffness) belongs to the specimen with cohesive failure mode including three steps with equal lengths (Design I). In detail, the overall stiffness in Design I is higher than the

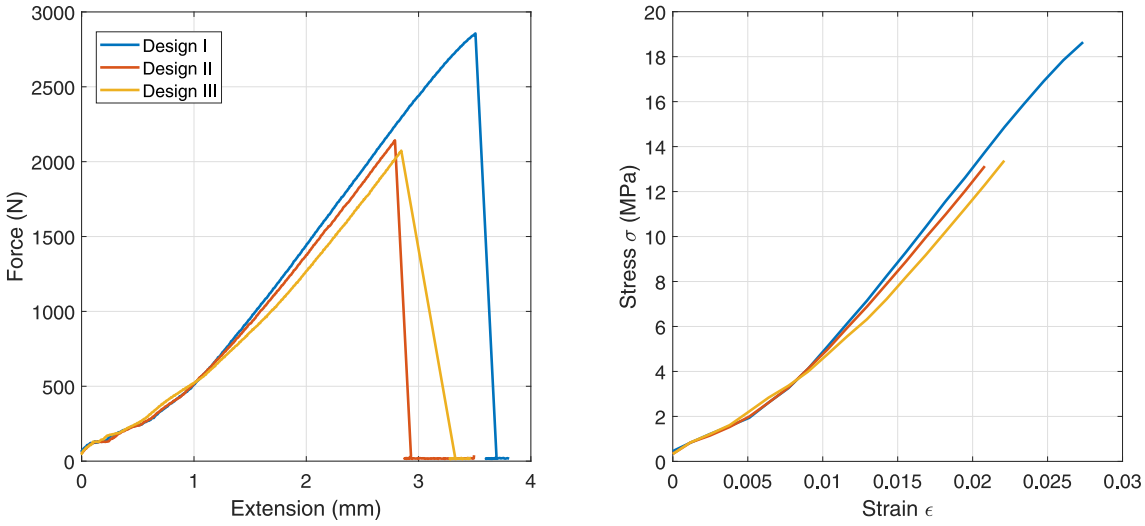

Fig. 7 – Force–displacement curves (left), and stress–strain curves (right) of the step-lap joints with different step configurations.

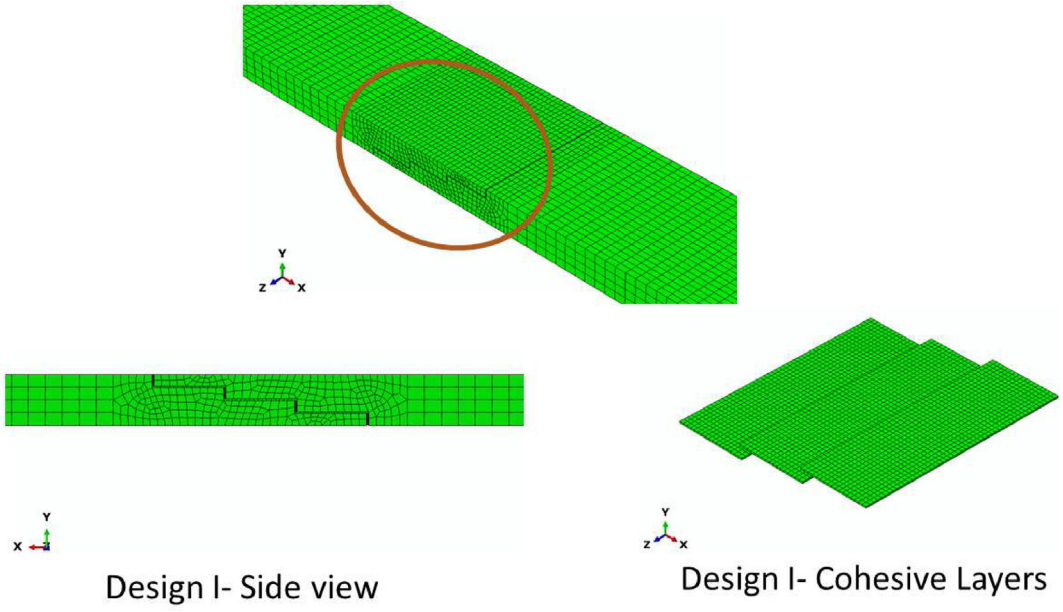

Fig. 8 – Finite element model of the adhesively bonded step-lap joint (Design I) including adhesive layers via CZM.

other two designs (it is about 1008 N/m), and it is reduced to 954 N/m in Design II.

In comparison with traditional single-lap joint studied in our previous research work [40], the present study proved that the structural integrity of adhesively bonded 3D-printed joint is increased by considering steps in overlap area. In detail, we reported the fracture load of 1986.2 N for traditional single lap joint in our previous study [40], but in the current study it has been increased to 2723.9 N for step-lap joint (Design I). In fact, comparison of results indicated that using step in overlap area leads to change in failure load of the joint, therefore, steps with equal length improve the mechanical performance and structural integrity of 3D-printed joints.

4. Computational approach

A computational finite element (FE) model was developed to investigate the effects of step-shaped bonding area with more depth on structural integrity of the joint specially from the stress distribution point of view. Having such a computational FE model provides a deeper understanding of stress and force transition between 3D-printed adherends and adhesive layers and demonstrates how topology of the bonding area leads to enhancement of the overall strength of the joint. We followed the same methodology in our previous publications in adhesively bonded 3D-printed joints with flat bonding area for PLA [40] and PETG [41] adherends. ABAQUS/Standard software was employed to create a nonlinear 3D-FE model of Design I (with identical step size) demonstrated in Fig. 4. Design I was chosen in FE model as it shows maximum fracture load amongst all three designs tested and reported via Table 2 and Fig. 7. A cohesive zone layer is considered for the adhesive layer in the joints using cohesive zone modelling elements (CZM) in ABAQUS. CZM enables the FE model to consider delamination in adhesive layer and to track adhesive failure in adhesively bonded joints. COH3D8 elements are employed to model the adhesive layer in which have been already used successfully to model other types of adhesively bonded joints [62–65]. We also employed the CZM in computational modelling of single lap adhesively bonded joints with different 3D-printed adherends [40,41]. The cohesive layer defines the fracture process and crack propagation within the adhesive and is modelled by the traction-separation law. Crack initiation in the adhesive layer is defined by the mixed-mode bilinear constitutive model [62], where both shear and normal cohesive strength of the adhesive, play role on damage initiation and crack growth. The 3D models of the step-lap adhesively bonded joint of Design I, is presented in Fig. 8 with their corresponding CZM of their adhesive layer. Material properties and strengths for the adhesive and PLA adherends are already defined in [40]. Mesh independency of the FE model has been already checked and the thickness of the cohesive layers is considered as 0.2 mm similar to the experimental samples stated in Table 1 and following the optimisation performed earlier in [40,41]. Material properties of 3D-printed PLA adherends were extracted from the experimental tensile test on the dumbbell-shaped test coupons printed with the same printing parameters and conditions as the adherends (Table 1) according to ASTM D638 [55]. Mechanical characteristics and parameters of the adhesive layer also were picked from the technical data-sheet of the adhesive (LOCTITE® EA 9466™ from Henkel), all abridged in Table 3.

To simulate the mechanical behaviours of the FE models similar to standard condition of the universal tensile test, detailed in Section 3, nodes located in one end of the FE model is assumed to be fixed while nodes at the other end experiences a gradual axial extension equal to *U*. The nonlinear FE static analysis is performed up to the fracture of the sample.

To demonstrate the accuracy of the FE model detailed in Fig. 8, variations of the axial force against the axial displacement *U* are plotted for both experimental tensile test and the FE model in Fig. 9. A good agreement is seen between the experimental results and the computational output of the FE model. Both graphs demonstrate a similar linear elastic pattern up to the fracture load, followed by a sharp decrease in the force due to the cohesive failure of the adhesive layers. The slope of the linear part of the graphs are proportional to the young modulus of the adherends (PLA) and the fracture

Table 3 – Mechanical properties of the PLA printed adherends and the adhesive.

Parameters	Values
Adherends	
Elastic Modulus (GPa)	0.77
Poisson ratio	0.33
Adhesive	
Shear strength (MPa)	37
Tensile strength (MPa)	32
Tensile modulus (GPa)	1.71
Impact strength (kJ/m^2)	5.1
Glass Transition Temperature (°C)	65

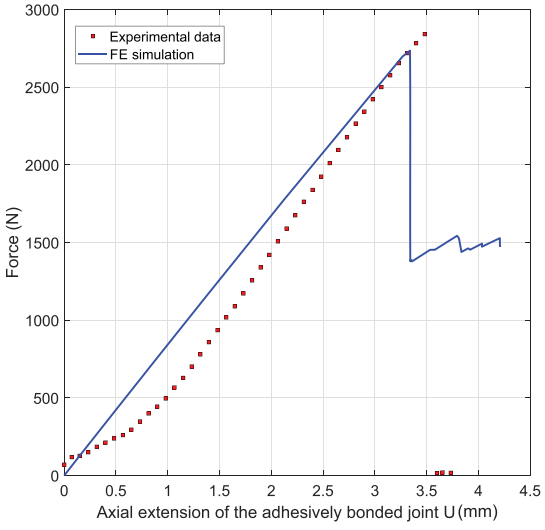

Fig. 9 – Force-displacement graph of the adhesively bonded sinle lap joint with stepped-lap bonding area (Design I) - a comparison between the experiment and the FE model.

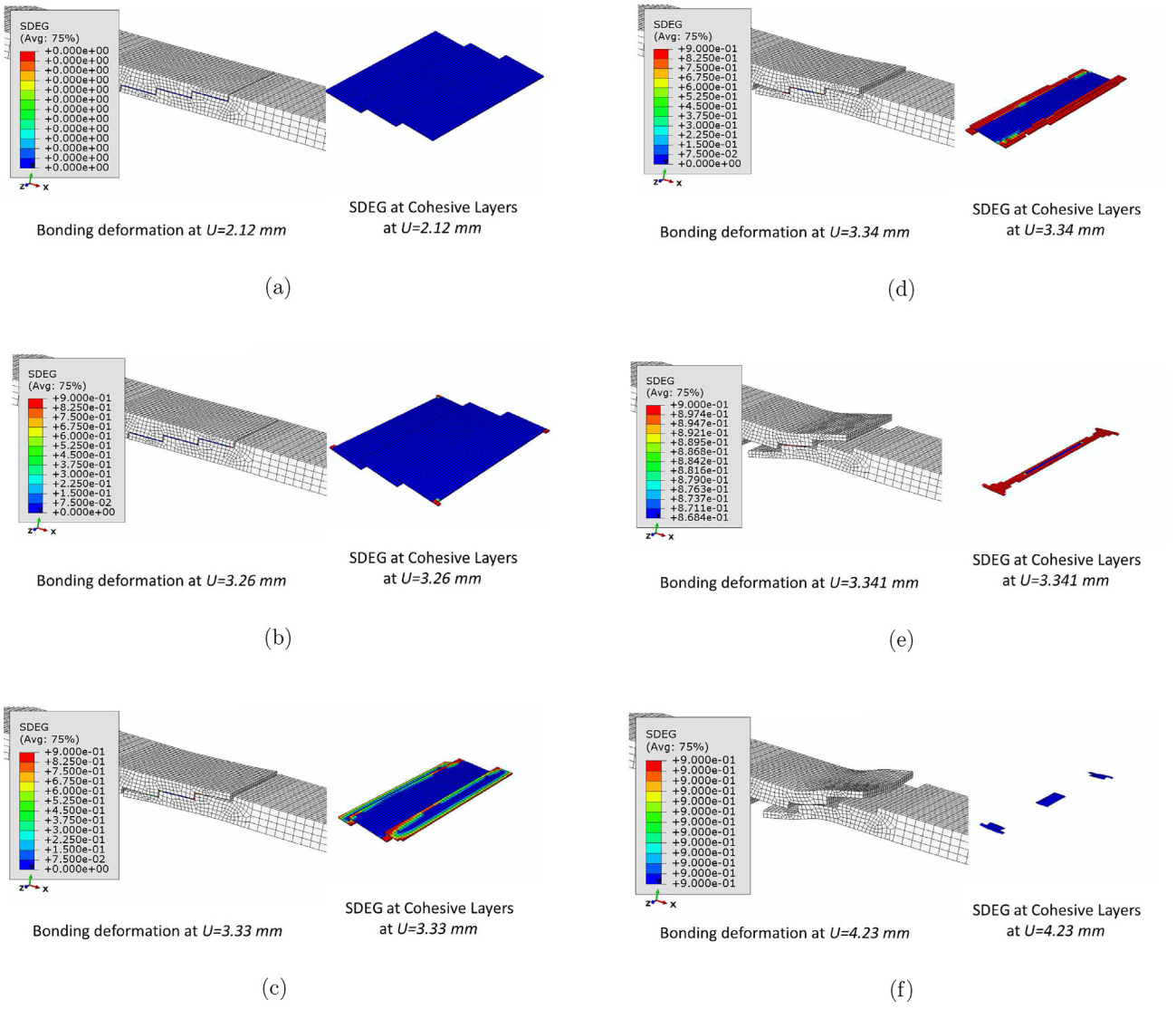

Fig. 10 – Damage evolution of the adhesively bonded joint at different extensional deformation *U*.

load in cohesive failure relates to the properties of the adhesive. The fracture load measured in the experimental test is recorded as $F_{max} = 2856$ N at $U = 3.5$ mm and the FE model predicts this force as $F_{max} = 2723$ N at $U = 3.35$ mm.

To explain the role of the adhesive layers in load transferring between the adherends, structural integrity of the joint and cohesive failure of the CZM layer; SDEG (scalar stiffness degradation) output of the cohesive zone layer in ABAQUS can be employed. SDEG output take values between zero and one and indicates the damage in cohesive elements in the adhesive layers. As the stress level inside the CZM gets closer to the maximum strength of the adhesive material, SDEG starts to approach from zero to one and when a CZM element is completely damaged, SDEG gets one and corresponding element(s) with SDEG = 1 will be deleted from the model. To analyse the evolution of the cohesive failure of the adhesively bonded step-lap joint with printed PLA adherends, deformation of the bonding zone along with SDEG variation on CZM layer at different axial deformations *U* are demonstrated in Fig. 10. From $U = 0$ up to $U = 2.12$ mm of axial extension, adhesive layers are not damaged and performing with full load transferring capacity. Fig. 10a shows the deformation of the bonding area (right picture) with SDEG value on adhesive layer (left picture) and it is shown that all CZM elements in adhesive layers are undamaged (i.e. SDEG = 0 for all elements). With further extension to values higher than $U = 2.12$ mm, adhesive layer starts to deteriorate and cohesive failure of adhesive begins. This cohesive failure starts from both the upper and the lower layer of the adhesive at their outer transverse edges. For instance, at $U = 3.26$ mm, first transverse row of the elements at the upper and lower adhesive layer have been almost damaged as shown in Fig. 10b and most of adhesive elements at these edges are deactivated and deleted. This adhesive deterioration leads to distributing more load to the remaining elements and materials in adhesive layers and cohesive failure accelerates with *U*, accordingly. At $U = 3.33$ mm (with just a 0.07 mm increase on *U* from the previous step) almost 50% of the adhesive material on the upper and lower layer of the CZM has been deteriorated and removed as seen in Fig. 10c. Moreover, at this stage the middle

layer also has started to fail from its outer transverse edges. At $U = 3.34$ mm (Fig. 10d), not only both the upper and the lower layer of the adhesive have been mostly deleted, but the middle layer also has lost 40% of its material. By increasing the extension to $U = 3.341$ mm (an increase of only 0.001 mm as seen in Fig. 10d), transverse layer of elements in the middle of the second step (middle layer) is the only element set which still has load transfer capacity. The adherends are almost detached as shown in Fig. 10e and the model are ruptured at $U = 4.23$ mm finally (Fig. 10e). Stress distribution across the axial directions of the adhesive layers are demonstrated in Fig. 11 and 12 at $U = 2.129$ mm and $U = 3.33$ mm, correspondingly.

Two axial paths are defined (one in the axial edge (path 1) and one in the middle axial line (path 2) of the adhesive layers) to record variation of different stress components via CZM and adhesive elements. At the extension $U = 2.129$ mm, where all adhesive elements are undamaged, von Mises stress variation on adhesive layers are given in Fig. 11a. Maximum von Mises stress occurs at the outer vertical edge of the upper and lower layers, where cohesive failure starts to grow and expand. However, the von Mises stress at the middle layer is almost negligible. In parallel, variation of the peel and shear stress components across path 1 and path 2 confirm the same concept. The peel and shear stress level, at both paths, next to the outer transverse edge is higher in both upper and lower layer, however, both peel/shear stress values in path 2 is slightly higher then path 1 close to the outer transverse edge. This is why element deterioration and cohesive failure start from the middle point of the outer transverse edge in the upper and lower layer toward the external axial edges. Moreover, at this loading stage, the peel/shear stress values in

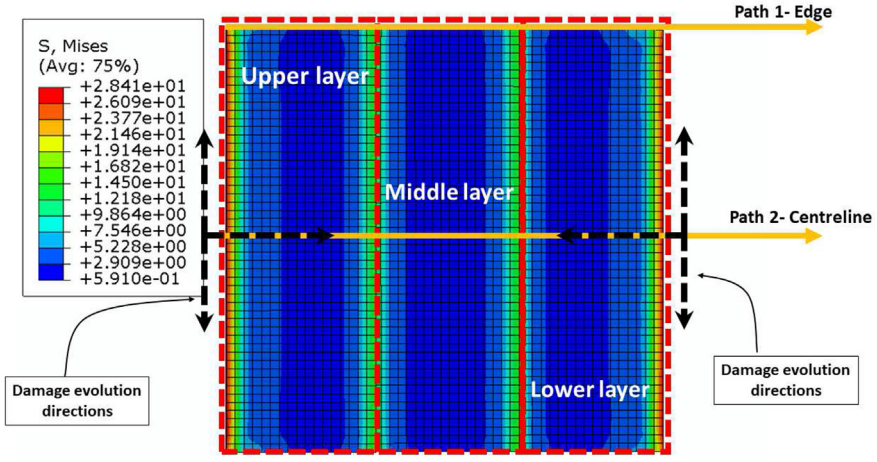

(a) Top view of the adhesive layers-von Mises stress distribution.

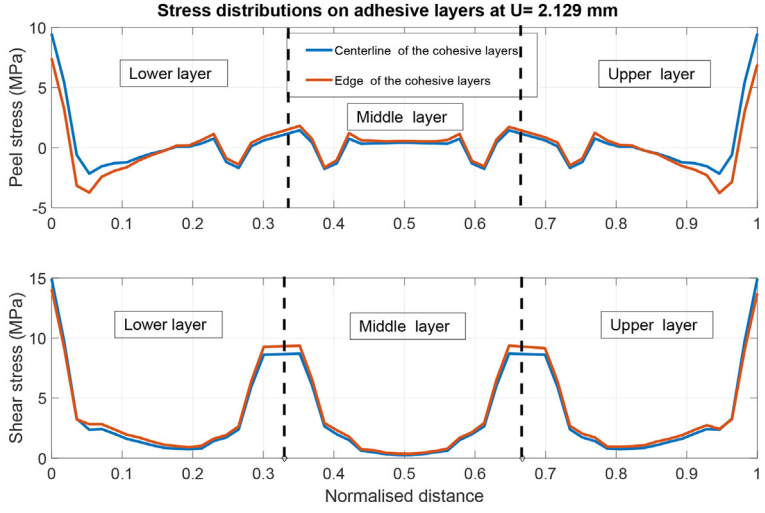

(b) Peel and shear stress variations on the centerline (path 1) and edgeline (path 2) of the adhesive layers at $U = 2.12$ mm.

Fig. 11 – Stress distributions on adhesive layers at U = 2.12 mm.

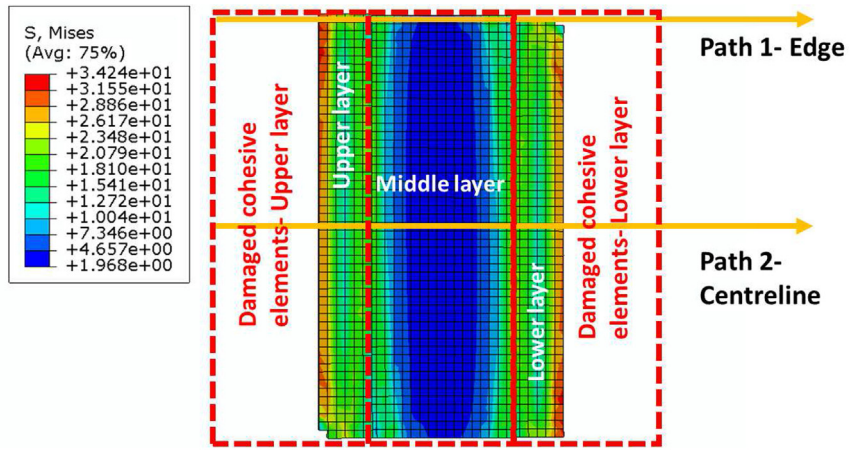

(a) Top view of the adhesive layers- von Mises stress distribution at $U = 3.33$ mm.

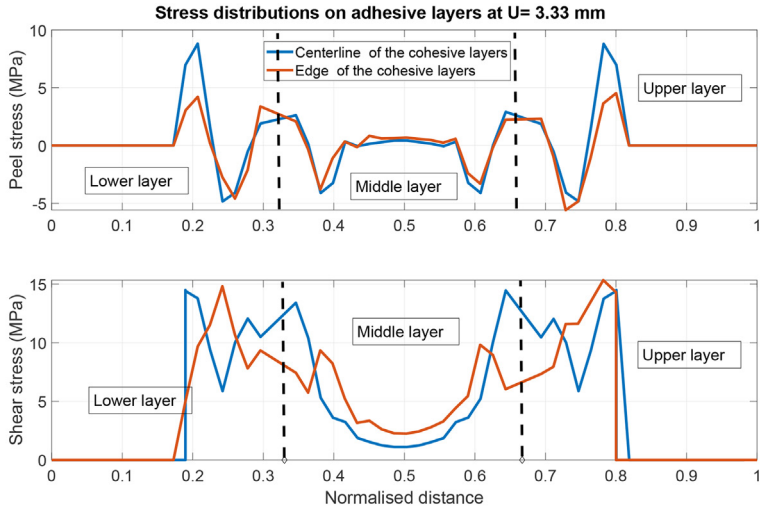

(b) Peel and shear stress variations on the centerline (path 1) and edgeline (path 2) of the adhesive layers at $U = 3.33$ mm.

Fig. 12 – Stress distributions on adhesive layers at $U = 3.33$ mm.

the middle layer are almost zero. Direction of the damage evolution on the adhesive layer is shown in Fig. 11a.

In Fig. 12a, stress distributions of adhesive layers are demonstrated at higher extension of $U = 3.33$ mm. As it was previously shown in Fig. 10c, almost 50% of the adhesive material in the upper and lower layer was deteriorated from their vertical outer edges and von Mises stress distribution shown in Fig. 12a confirm that the damage evolution pattern is still the same as $U = 2.12$ mm Maximum von Mises stress happens at vertical external edges of the upper and lower layer and according to the peel/shear stress distribution on path 1 and 2 (in Fig. 12b), maximum stress still occurs at the middle points of external vertical edges at the upper and lower layer. And cohesive failure is growing from the middle point of the upper and lower layer toward the axial edges and toward the internal transverse edge of these layers.

5. Discussion

'Experimental practices indicated that steps in overlap area can increase fracture load and improve structural integrity of the 3D-printed joint. In addition, experiments showed that cohesive failure was occurred in most of the examined joints (nine out of twelve specimens). Although we have considered three different designs in step-lap joints (steps with different lengths and configurations), only Designs I shows significant improvement in fracture load and mechanical performance of the joint. Comparison of the results indicated that change in the step length changes the failure load and the displacement capacity of the joint. When the first step length is decreased from 8.5 mm to 3 mm, the displacement of the joint and its failure load decreased. Moreover, the area under the force-

displacement curve shows the energy absorbed by the connection. In this context, the energy of the joint in Design I is large, while the energy of Design II and Design III is approximately equal to each other.

In adhesively bonded joints, the peel stresses that occur at the ends of the overlap area, because of eccentric loading form a crack at the ends of the overlap area, and damage is caused by propagation of this crack towards the center of the overlap area. In step-lap joints sudden progress of the crack towards the center can be prevented due to the step in the overlap area. In our previous research on additively manufactured joint, we have reported effective stress of 3.07 MPa for traditional PLA 3D-printed single lap joint, but it has been increased 23% and reached to 3.7 MPa in step-lap joint (Design I). The 3D nonlinear FE computational model developed for Design I, also confirms what was revealed in the experiments. The FE model showed that the cohesive failure on the adhesive layer starts at the outer transverse edge of the upper and lower layer from their middle points and this failure occurs around the axial extension around $U = 2.12$ mm. This cohesive failure rapidly propagates toward the center of the adhesive layer and the transverse edges (as shown in Fig. 11a). It is also demonstrated failure in adhesive layers at top and bottom step rapidly grows with U and cause cohesive damage in the middle layer within just few micro-millimeter increase in extension. The middle layer carries high level of stress afterward leading to complete and rupture of the bonded structure.

6. Conclusion

Based on simplicity and benefits of FDM process, a growing list of companies have commercialized this technique for a wide spectrum of materials. Therefore, structural integrity and mechanical performance of 3D-printed parts are became of importance. In the present study, we have considered steps with different lengths in overlap area of single lap joints. PLA material was used for fabricate step-lap joints based in the FDM process. A series of experiments was carried out to determine fracture load and mechanical performance of the joints. The bonding area is considered to be in the step-lap form and three different designs with different step sizes were manufactured and tested. The adhesive layer thickness was assumed to be identical in all samples and was considered as 0.2 mm as the optimised thickness we found in our previous research. The experiments reveal that amongst different step sizes considered in this study, the one with identical step size (so called Design I in Fig. 4) shows the highest fracture load and structural toughness and can be considered as the optimised shape design of the bonding area. A 3D nonlinear FE model of Design I was also developed to investigate the structural integrity of this adhesively bonded structure with PLA printed adherends. The model reveals the details of cohesive failure of Design I. The model confirms that the cohesive damage starts from the middle point of the outer transverse edge of the upper and the lower adhesive layer in design I and the damage quickly propagates toward the external axial edges and also toward the center of these layer with extension of the sample. Once both the upper and the lower adhesive layer fails, the central (middle) adhesive layer of the bond carries a high level of stress and this leads to a sudden failure of this layer and rupture of the whole bonded structure.

Declaration of Competing Interest

The authors declare that they have no known competing financial interests or personal relationships that could have appeared to influence the work reported in this paper.

Acknowledgements

This work as part of the project “Smart Production Design Center” (SmaP) is funded by the European Regional Development Fund (ERDF) under the program OP EFRE NRW 2014–2020 (EFRE-0200545).

EUROPÄISCHE UNION
Investition in unsere Zukunft
Europäischer Fonds
für regionale Entwicklung

EFRE.NRW
Investitionen in Wachstum
und Beschäftigung

REFERENCES

[1] Gibson I, Rosen D, Stucker B, Khorasani M. Additive manufacturing technologies. Springer; 2021.
[2] Stano G, Percoco G. Additive manufacturing aimed to soft robots fabrication: a review. Extreme Mech. Lett. 2021;42:101079.
[3] Higgins M, Leung S, Radacsi N. 3D printing surgical phantoms and their role in the visualization of medical procedures. Ann 3D Print Med 2022;6:100057.
[4] Khosravani MR, Reinicke T. 3D-printed sensors: current progress and future challenges. Sens Actuators, A 2020;305:111916.
[5] Nascimento DL, Neopomuceno RM, Caiado RG, Maqueira JM, Fuentes JM, Reyes JA. A sustainable circular 3D printing model for recycling metal scrap in the automotive industry. J Manuf Technol Manag 2022;33:876–92.
[6] Khosravani MR, Haghighi A. Large-scale automated additive construction: overview, robotic solutions, sustainability, and future prospect. Sustainability 2022;14:9782.
[7] Mantihal S, Kobun R, Lee BB. 3D food printing of as the new way of preparing food: a review. Int. J. Gastron. Food Sci. 2020;22:100260.
[8] Dagkolu A, Gokdag I, Yilmaz O. Design and additive manufacturing of a fatigue-critical aerospace part using topology optimization and L-PBF process. Procedia Manuf 2021;54:238–43.
[9] Wang J, Wu B, Liu G, Bu T, Guo T, Pang Y, et al. Flexure hinges based triboelectric nanogenerator by 3D printing. Extreme Mech. Lett. 2018;20:38–45.
[10] Montgomery SM, Hilborn H, Hamel CM, Kuang X, Long KN, Qi HJ. The 3D printing and modeling of functionally graded kelvin foams for controlling crushing performance. Extreme Mech. Lett. 2021;46:101323.
[11] Sajjadi SA, Ghasemi FA, Rajaee P, Fasihi M. Evaluation of fracture properties of 3d printed high impact polystyrene

according to essential work of fracture: effect of raster angle. Addit Manuf 2022;59:103191.
[12] Xue T, Wallin TJ, Menguc Y, Adriaenssens S, Chiaramonte M. Machine learning generative models for automatic design of multi-material 3D printed composite solids. Extreme Mech. Lett. 2020;41:100992.
[13] Rahmatabadi D, Ghasemi I, Baniasadi M, Abrinia K, Bagheri M. 3D printing of PLA-TPU with different component ratios: fracture toughness, mechanical properties, and morphology. J Mater Res Technol 2022;21:3970–81.
[14] Son KT, Phan TQ, Levine LE, Kim KS, Lee K, Ahlfors M, et al. The creep and fracture properties of additively manufactured inconel 625. Materialia 2021;15:101021.
[15] Zhang C, Xu S, Liu J, Ma Y. Comprehensive clustering-based topology optimization for connectable multi-scale additive manufacturing structures. Addit Manuf 2022;54:102786.
[16] Khodashenas H, Mirzadeh H. Post-processing of additively manufactured high-entropy alloys - a review. J Mater Res Technol 2022;21:3795–814.
[17] Liu F, Li T, Jia Z, Wang L. Combination of stiffness, strength, and toughness in 3D printed interlocking nacre-like composites. Extreme Mech. Lett. 2020;35:100621.
[18] Chen SG, Gao HJ, Zhang YD, Wu Q, Gao ZH, Zhou X. Review on residual stresses in metal additive manufacturing: formation mechanisms, parameter dependencies, prediction and control approaches. J Mater Res Technol 2022;17:2950–74.
[19] Harris JA, Winter RE, McShane GJ. Impact response of additively manufactured metallic hybrid lattice materials. Int J Impact Eng 2017;104:177–91.
[20] Lee KH, Yun GJ. Design optimization of thermally conductive support structure for laser powder-bed fusion process with part-scale thermal history. Addit Manuf 2022;51:102627.
[21] ASTM F2792 - 12 Standard Terminology for Additive Manufacturing Technolo-gies, Standard. West Conshohocken, USA: American Society for Testing Materials; 2012.
[22] Tiwary VK, Arunkumar P, Malik VR. An overview on joining/welding as post-processing technique to circumvent the build volume limitation of an fdm-3d printer. Rapid Prototyp J 2021;27:808–21.
[23] Dillard DA. Advances in structural adhesive bonding. Elsevier; 2010.
[24] Cavezza F, Boehm M, Terryn H, Hauffman T. A review on adhesively bonded aluminium joints in the automotive industry. Metals 2020;10(6):730.
[25] Sarkar R, Chen B, Fitzpatrick ME, Fabijanic D, Hildtich T. Additive manufacturing-based repair of IN718 superalloy and high-cycle fatigue assessment of the join. Addit Manuf 2022;60:103276.
[26] Shishesaz M, Hosseini M. Effects of joint geometry and material on stress distribution, strength and failure of bonded composite joints: an overview. J Adhes 2018;96:1053–121.
[27] Shang X, Marques E, Machado J, Carbas R, Jiang D, Da Silva L. Review on techniques to improve the strength of adhesive joints with composite adherends. Composites, Part B 2019;177:107363.
[28] Kupski J, de Freitas ST. Design of adhesively bonded lap joints with laminated CFRP adherends: review, challenges and new opportunities for aerospace structures. Compos Struct 2021;268:113923.
[29] Yousefi Kanani A, Green S, Hou X, Ye J. Hybrid and adhesively bonded joints with dissimilar adherends: a critical review. J Adhes Sci Technol 2021;35(17):1821–59.
[30] Huang ZC, Jia YL, Jiang YQ, Zhang YC. Mechanical properties and fatigue failure mechanisms of purely self-piercing riveted (SPR) and hybrid (SPR-bonded) joints under salt spray environment. J Mater Res Technol 2022;20:2501–17.
[31] Kumazawa H, Kasahara T. Analytical investigation of thermal and mechanical load effects on stress distribution in adhesive layer of double-lap metal-composite bonded joints. Adv Compos Mater 2019;28(4):425–44.
[32] Rangaswamy H, Sogalad I, Basavarajappa S, Patel GM. Experimental analysis and prediction of strength of adhesive-bonded single-lap composite joints: taguchi and artificial neural network approaches. Microsc Microanal 2015;21:15.
[33] Gualberto HR, do Carmo Amorim F, Costa HRM. A review of the relationship between design factors and environmental agents regarding adhesive bonded joints. J Braz Soc Mech Sci Eng 2021;43(8):1–19.
[34] Wu C, Chen C, He L, Yan W. Comparison on damage tolerance of scarf and stepped-lap bonded composite joints under quasi-static loading. Composites, Part B 2018;155:19–30.
[35] Durmuş M, Akpinar S. The experimental and numerical analysis of the adhesively bonded three-step-lap joints with different step lengths. Theor Appl Fract Mech 2020;105:102427.
[36] Khashaba U, Najjar IM, Almitani KH. Failure analysis of scarf adhesive joints modified with sic-nanoparticles under fatigue loading at room temperature. Compos Sci Technol 2022;221:109301.
[37] Alves D, Campilho R, Moreira R, Silva F, Da Silva L. Experimental and numerical analysis of hybrid adhesively-bonded scarf joints. Int J Adhesion Adhes 2018;83:87–95.
[38] Cavalcanti D, Banea M, Queiroz H. Mechanical characterization of bonded joints made of additive manufactured adherends. Annals of "Dunarea de Jos" University of Galati. Fascicle XII, Welding Equipment and Technology 2019;30:27–33.
[39] Spaggiari A, Denti F. Mechanical strength of adhesively bonded joints using polymeric additive manufacturing. Proc Inst Mech Eng, Part C: J Mech Eng Sci 2021;235(10):1851–9.
[40] Khosravani MR, Soltani P, Weinberg K, Reinicke T. Structural integrity of adhesively bonded 3D-printed joints. Polym Test 2021;100:107262.
[41] Khosravani MR, Soltani P, Reinicke T. Fracture and structural performance of adhesively bonded 3D-printed PETG single lap joints under different printing parameters. Theor Appl Fract Mech 2021;116:103087.
[42] Barbosa NGC, Campilho RDSG, Silva FJG, Moreira RDF. Comparison of different adhesively-bonded joint types for mechanical structures. Appl. Adhes. Sci. 2018;6:1–19.
[43] da Silva LFM, Critchlow GW, Figueiredo MAV. Parametric study of adhesively bonded single lap joints by the taguchi method. J Adhes Sci Technol 2008;22:1477–94.
[44] Liu Z, Minsky H, Creton C, Ciccotti M, Hui CY. Mechanics of zero degree peel test on a tapee - effects of large deformation, material nonlinearity, and finite bond length. Extreme Mech. Lett. 2019;32:100518.
[45] Shang X, Marques EAS, Carbas RJC, Barbosa AQ, Jiang D, da silva LFM, et al. Fracture mechanism of adhesive single-lap joints with composite adherends under quasi-static tension. Compos Struct 2020;251:112639.
[46] Sun F, Pruncu CI, Penchev P, Jiang J, Dimov S, Blackman BRK. Influence of surface micropatterns on the mode i fracture toughness of adhesively bonded joints. Int J Adhesion Adhes 2020;103:102718.
[47] Dumont V, Stamoulis G, Badulescu C, Lefevre A, Thevenet D. Investigation of the influence of the temperature on the fracture properties of adhesive joints using the Arcan device. Int J Adhesion Adhes 2022;269:108524.
[48] da Silva LFM, Lopes MJC. Joint strength optimization by the mixed-adhesive technique. Int J Adhesion Adhes 2009;29:509–14.

[49] Vogelesang LB, Vlot A. Development of fibre metal laminates for advanced aerospace structures. J Mater Process Technol 2000;103:1–5.
[50] Shang X, Marques EAS, Machado JJM, Carbas RJC, da Silva DJLFM. A strategy to reduce delamination of adhesive joints with composite substrates. Proc. Inst. Mech. Eng. L. J. Mater. Des. Appl. 2019;233:521–30.
[51] Bilsik K. Three-dimensional braiding for composites: a review. Textil Res J 2013;83:1414–36.
[52] Bogdanocih AE, Dannemann M, Döell J, Leschik T, Singleatry JN, Hufenbach WA. Experimental study of joining thick composites reinforced with non-crimp 3D orthogonal woven e-glass fabrics. Composites, Part A 2011;42:896–905.
[53] Mouritz AP. Review of z-pinned composite laminates. Composites, Part A 2007;38:2383–97.
[54] Chan W. Design approaches for edge delamination resistance in laminated composites. J Compos Technol Res 1991;13:91–6.
[55] ASTM D638 -14 Standard Test Method for Tensile Properties of Plastics, Standard. West Conshohocken, USA: American Society for Testing Materials; 2014.
[56] Datasheet P.L.A. https://docs.rs-online.com/f1a8/0900766b81698003.pdf accessed: 03.06.2022.
[57] ASTM D3163 -01 determining strength of adhesively bonded rigid plastic lap-shear joints in shear by tension loading, standard. West Conshohocken, USA: American Society for Testing Materials; 2001.
[58] Ebnesajjad S. Surface treatment of materials for adhesive bonding. Elsevier; 2014.
[59] Khosravani MR. Influences of defects on the performance of adhesively bonded sandwich joints. Key Eng Mater 2018;789:45–50.
[60] Petrie EM. Plastics and adhesives as adhesives. McGraw-Hill; 1975.
[61] Cagle CV. Adhesive bonding, techniques and applications. McGraw-Hill; 1968.
[62] Barzegar M, Moallem MD, Mokhtari M. Progressive damage analysis of an adhesively bonded composite t-joint under bending, considering micro-scale effects of fiber volume fraction of adherends. Compos Struct 2021;258:113374.
[63] Hosseini-Toudeshky H, Sheibanian F, Ovesy HR, Goodarzi MS. Prediction of interlaminar fatigue damages in adhesively bonded joints using mixed-mode strain based cohesive zone modeling. Theor Appl Fract Mech 2020;106:102480.
[64] He X. A review of finite element analysis of adhesively bonded joints. Int J Adhesion Adhes 2011;31(4):248–64.
[65] Budhe S, Banea M, De Barros S, Da Silva L. An updated review of adhesively bonded joints in composite materials. Int J Adhesion Adhes 2017;72:30–42.